ISIJ International, Vol. 32 (1992), No. 4, pp. 496–504

Reduction Kinetics of Cement-bonded Natural Ilmenite Pellets with Hydrogen

Kang SUN, Reijiro TAKAHASHI and Jun-ichiro YAGI

Research Institute of Mineral Dressing and Metallurgy, Tohoku University, Katahira, Aoba-ku, Sendai, Miyagi-ken, 980 Japan.

(Received on September 17, 1991; accepted in final form on December 20, 1991)

The hydrogen reduction kinetics of ilmenite was studied thermogravimetrically from 1 073 to 1 273 K with three kinds of cement-bonded natural ilmenite pellets. The kinetic behavior of the reduction of preoxidized ilmenite was researched with the same technique from 973 to 1 273 K. The reduction of the pellets proceeded topochemically, but, the behavior of the grains constituting the pellets was more complex. The reduction kinetics of preoxidized pellets was analyzed according to a two-interface kinetic model and the kinetic parameters of the two main reactions $Fe^{3+} \rightarrow Fe^{2+}$ and $Fe^{2+} \rightarrow Fe^{\circ}$, which mainly constitute the overall reduction of preoxidized ilmenite pellets, were determined separately. The experimental data of the reduction of unoxidized pellets were interpreted in terms of a modified one-interface kinetic model derived from the aforementioned two-interface kinetic model. Diffusion of gaseous species through product layer and intrinsic chemical reaction were found to be the main rate controlling factors during reduction.

KEY WORDS: kinetics; hydrogen reduction; natural ilmenite; cement-bonded pellet; thermogravimetry; two-interface kinetic model; rate-controlling step.

1. Introduction

Study on the reduction of ilmenite started as early as 1910 s[1] and since then, it has been both widely and deeply extended[1-14] because of its importance of this step in upgrading the titanium concentrate. However, the reduction kinetics especially the kinetic behavior of the ferric material is still not very clear, requiring further research.

This work was designed in a somewhat different way from previous reports,[9-11] that is, cement-bonded ilmenite pellets consisted of different substances, such as $FeTiO_3$, $Fe_2Ti_3O_9$ and Fe_2TiO_5 *etc.*, were prepared in advance, and then the reduction kinetics of each kind of pellet was studied with hydrogen individually. Moreover, the measured data were analyzed in the light of a two-interface kinetic model so as to clarify the kinetic behavior of each of the two main steps concerned, namely, the conversion of the ferric material in the preoxidized ilmenite pellets to ferrous material and the further reduction of the ferrous material formed to metallic iron.

2. Experimental

2.1. Apparatus and Procedure

The reduction kinetics of cement-bonded natural ilmenite pellets was studied thermogravimetrically with the same apparatus described previously[15] by using pure hydrogen. The inner diameter of the reactor was 50 mmϕ and the uniform temperature zone within ± 2 K was about 20 cm in height. The gas flow rate was controlled at 1.67×10^{-4} m^3/s (NTP). The reduction of preoxidized ilmenite pellets was carried out from 973 to 1 273 K. Because the reduction rate of unoxidized ilmenite pellets was obviously slow when temperature was 973 K, the reduction of unoxidized ilmenite pellets was conducted from 1 073 to 1 273 K.

In order to prevent the reduced pellet from being oxidized again, when the reduction finished, it was quenched at water-cooling part under nitrogen atmosphere for more than 1.8 ks.

The mineral composition of the samples was analyzed by means of X-ray diffraction (XRD) and the structure of the partially reduced pellets was examined by EPMA and optical microscopy.

2.2. Samples

Three kinds of natural ilmenite ores from Australia, China and Malaysia were used for making the cement-bonded pellets.[15] Their chemical composition and size distribution after crushing were given previously.[15] According to the XRD results, they mainly consisted of $FeTiO_3$. The cement-bonded pellets containing 8.0 mass% of Portland cement were prepared

Table 1. Density and porosity of the dehydrated pellets.

Pellets	ACP	CCP	MCP
Apparent density $\rho_{a2} \times 10^{-3}$ (kg·m^{-3})	3.12	3.17	3.02
True density $\rho_{s2} \times 10^{-3}$ (kg·m^{-3})	4.26	4.32	4.35
Porosity ε_2 (−)	0.268	0.266	0.306

Table 2. Density and porosity of the pellets preoxidized at 1073 and 1273 K.

Pellets	ACP		CCP		MCP	
Preoxidation temperature (K)	1073	1273	1073	1273	1073	1273
Apparent density $\rho_{a1} \times 10^{-3}$ (kg·m^{-3})	3.22	3.05	3.09	3.11	3.15	3.08
True density $\rho_{s1} \times 10^{-3}$ (kg·m^{-3})	4.32	4.20	4.40	4.09	4.30	4.07
Porosity ε_1 (−)	0.255	0.274	0.298	0.240	0.267	0.243

with a disk pelletizer which was 30 cm in diameter. Green pellets were cured under saturated water vapor atmosphere at 323 K for one week, then dried at 373 K in air for two days and finally dehydrated at 1173 K under oxygen-free nitrogen atmosphere for 1 h. Their strength was over 100 kg per pellet. Preliminary test showed that combined water was removed sufficiently by the above-mentioned treatment. For simplicity, hereafter, the three kinds of pellets made of ilmenite ores from Australia, China and Malaysia will be designated as ACP, CCP and MCP, respectively. The pellet size is from 12.5 to 13.0 mm in diameter and their density and porosity after dehydration are given in **Table 1**.

Because their kinetic behavior was similar, only the results measured with ACP will be mainly presented here.

In order to examine the effect of preoxidation on the subsequent reduction kinetics, some pellets which had been dried at 373 K were preoxidized at 1073 or 1273 K, respectively, with pure O_2 for 2 h. According to the results of XRD, the preoxidation was complete under such conditions and the pellets preoxidized at 1073 K mainly consisted of $Fe_2Ti_3O_9$ and Fe_2O_3 and those preoxidized at 1273 K were mainly composed of Fe_2TiO_5 and TiO_2. The density and porosity of the preoxidized pellets are given in **Table 2**.

3. Experimental Results and Theoretical Analysis

3.1. Outline of the Reduction

3.1.1. Reactions

According to the results of XRD measured before and after reduction, the main reduction reaction of the unoxidized pellets can be stoichiometrically expressed as Eq. (1):

$$FeTiO_3 + H_2 = Fe + TiO_2 + H_2O \quad \text{.....(1)}$$

The principal reactions of the reduction of pellets preoxidized at 1073 K can be described as follows:

$$1/3\,Fe_2Ti_3O_9 + H_2 = 2/3\,Fe + TiO_2 + H_2O \quad \text{.....(2)}$$

and

$$1/3\,Fe_2O_3 + H_2 = 2/3\,Fe + H_2O \quad \text{.....(3)}$$

The main reaction of the reduction of pellets preoxidized at 1273 K is expressed by the following formula:

$$1/3\,Fe_2TiO_5 + H_2 = 2/3\,Fe + 1/3\,TiO_2 + H_2O \quad \text{.....(4)}$$

Figure 1 illustrates the effect of preoxidation on the subsequent reduction rate, showing that preoxidation accelerates the following reduction.

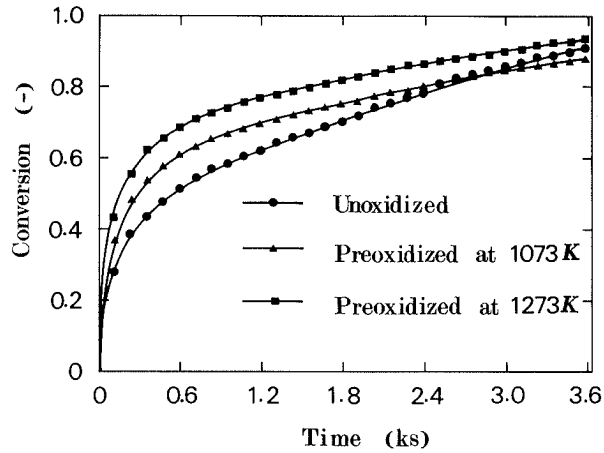

Fig. 1. Effect of preoxidation on the subsequent reduction rate during the reduction of ACP at 1173 K.

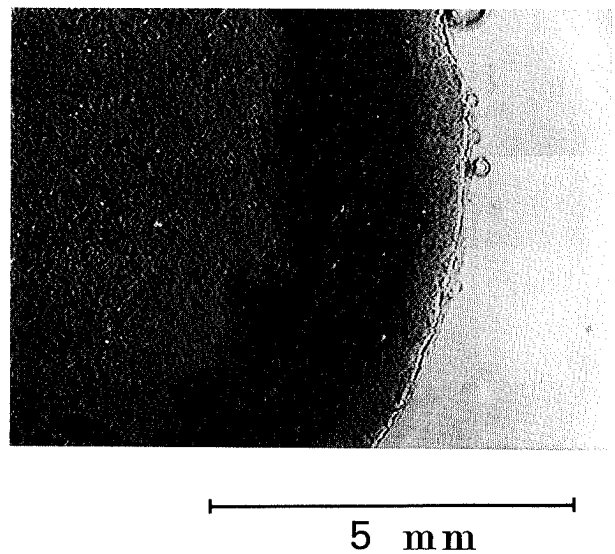

Fig. 2. Photograph of partially reduced ACP (x=0.5) at 1073 K showing that the reduction proceeded topochemically with two reaction interfaces.
unreacted core: $Fe_2TiO_5 + TiO_2$, first product layer: $FeTiO_3 + TiO_2$, second product layer: $Fe + TiO_2$

3.1.2. Reaction Sequence

The reaction mechanism of the reduction of natural ilmenite is very complicated and changes as reaction proceeds.[5-7] The reduction sequence of oxidized (or well weathered) ilmenite can be principally summarized and simply expressed as the following two steps[5]:

(a) the conversion of ferric material into ferrous material:

$$Fe^{3+} \longrightarrow Fe^{2+}$$

(b) the reduction of the ferrous material to metallic iron:

$$Fe^{2+} \longrightarrow Fe^{\circ}$$

and the further reduction of TiO_2 to titanium suboxide.

As pointed out by Jones,[5] step (a) proceeds more easily compared to step (b). Because of the lack of thermodynamic properties of some complex compounds, such as $Fe_2Ti_3O_9$ and Fe_2TiO_5, in the following analysis, reaction occurring in step (a) will be approximately treated as reaction (I).

Reaction (I): $Fe_2O_3 + H_2 = 2FeO + H_2O$

and reaction occurring in step (b) can be expressed as

Reaction (II): $FeTiO_3 + H_2 = Fe + TiO_2 + H_2O$

According to the XRD results of the reduced pellets, the characteristic peaks of titanium suboxide are relatively weak, the effect of the further reduction of TiO_2 will be neglected in the following discussion.

3.1.3. Reaction Mode of the Pellets

As shown in **Fig. 2**, the cross-section of the partially reduced pellet reveals two distinctive boundaries between reduced layers and the unreacted core. This phenomenon indicates that, macroscopically, the reduction of the pellet proceeded topochemically under the experimental conditions. However, the reduction of each grain constituting the pellets did not proceed so simply. **Figure 3** compares the structure of the grains before and after reduction. It shows that, after reduction, the metallic iron (bright parts) separated from oxides (gray parts) which mainly consisted of TiO_2. The distribution of Ti and Fe after reduction was shown in **Fig. 4**. In the following discussion, the reduction kinetics will be analyzed in terms of the behavior of the pellet and little attention will be paid to each grain.

During the reduction of preoxidized pellets, it was the stepwise reaction mechanism and the two steps proceeding at different reaction rates that caused the reaction mode of the pellets changing from two interfaces to one interface as reduction proceeded. During the first period, reactions (I) and (II) proceeded simultaneously, and because the rate of reaction (I) was faster than that of reaction (II), there were two reaction interfaces. The

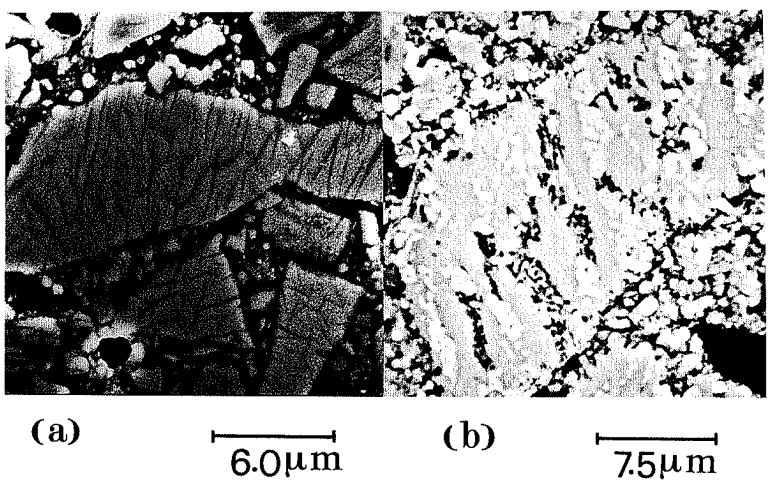

Fig. 3.
Comparison of the structure of original ilmenite grains with that of reduced ones.
(a) original ilmenite, gray parts are rich in iron, dark parts are rich in titanium.
(b) reduced ilmenite, bright parts are metallic iron and gray parts are oxides.

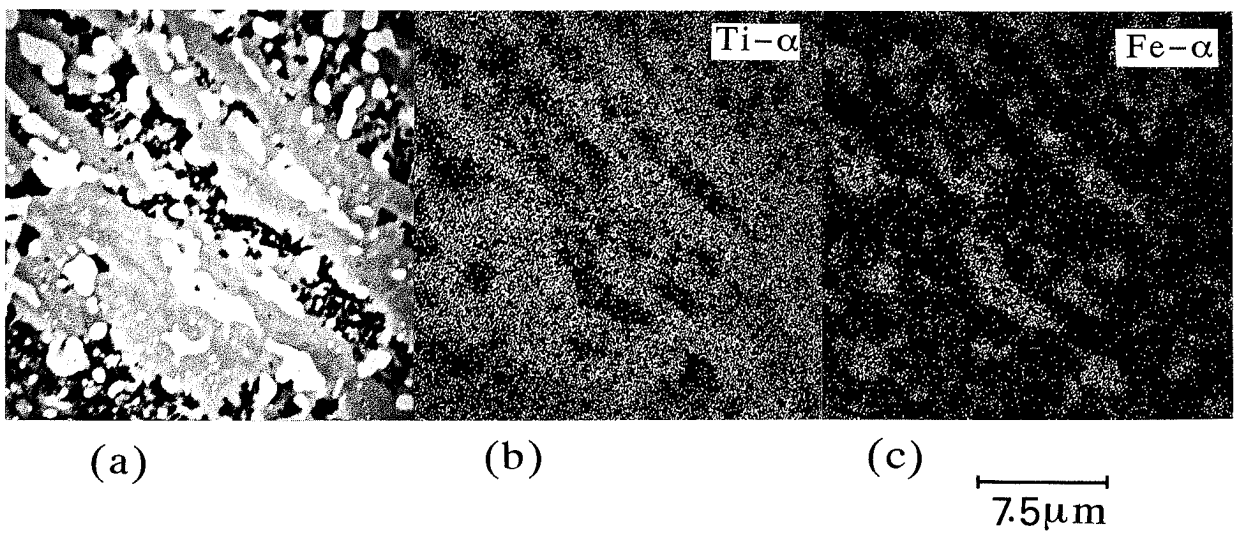

Fig. 4. Photograph of EPMA for ACP reduced at 1273 K after preoxidation at 1073 K.
(a) photomicrograph of reduced grains showing that metallic iron (bright parts) separated from oxides (gray parts)
(b) distribution of titanium
(c) distribution of iron

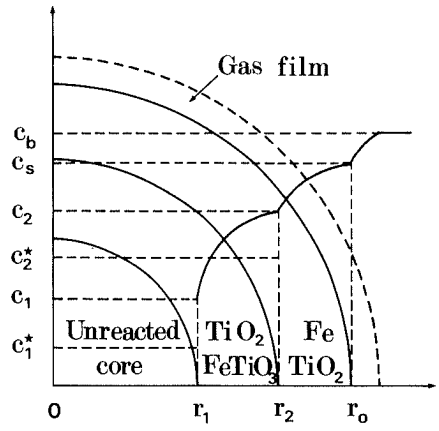

Fig. 5. Schematic diagram of the two-interface reaction system.

overall conversion measured was the combined contribution of both of them. In the second stage, however, reaction (I) finished and only reaction (II) continued. Consequently, the reacting pellet became a one-interface system.

3.2. Two-interface Kinetic Model

As shown in Fig. 2, during the initial period of the reduction of oxidized ilmenite pellets, the reacting pellet revealed two reaction interfaces. For easy understanding, the two-interface reaction system was schematically illustrated in **Fig. 5**. Based on the pseudo-steady state approximation and assuming that the activities of the solid reactant and product equal unity, the two-interface kinetic model can be derived as follows.

The shrinking rate of the two interfaces can be expressed as Eqs. (5) and (6), respectively.

$$\frac{d\xi}{d\theta_1} = -\gamma_1 \cdot \frac{\lambda_{c1}[\lambda_{c2}(1-\phi_2^*)+(\lambda_f+\lambda_{d2}+\lambda_{c2})(\phi_2^*-\phi_1^*)]}{[(\lambda_f+\lambda_{d2})(\lambda_{d1}+\lambda_{c1}+\lambda_{c2})+\lambda_{c2}(\lambda_{d1}+\lambda_{c1})](1-\phi_1^*)} \quad \text{.....(5)}$$

$$\frac{d\zeta}{d\theta_2} = -\gamma_2 \cdot \frac{\lambda_{c2}[(\lambda_{d1}+\lambda_{c1})(1-\phi_1^*)+(\lambda_f+\lambda_{d1}+\lambda_{d2}+\lambda_{c1})(\phi_1^*-\phi_2^*)]}{[(\lambda_f+\lambda_{d2})(\lambda_{d1}+\lambda_{c1}+\lambda_{c2})+\lambda_{c2}(\lambda_{d1}+\lambda_{c1})](1-\phi_2^*)} \quad \text{.....(6)}$$

Their initial conditions are given by Eq. (7).

$$\xi=\zeta=1\,, \quad \text{when} \quad \theta_1=\theta_2=0 \quad \text{.....(7)}$$

When reaction (I) finished, the reduction of the pellet became a one-interface system which was described by Eqs. (8) and (9).

$$\xi=0\,, \qquad \theta_1 \geq \theta_{1,c} \quad \text{.....(8)}$$

$$\frac{d\zeta}{d\theta_2} = -\gamma_2 \frac{\lambda_{c2}}{(\lambda_f+\lambda_{d2}+\lambda_{c2})} \quad \text{.....(9)}$$

with the initial condition expressed by Eq. (10).

$$\zeta=\zeta_c\,, \quad \text{when} \quad \theta_2=\theta_{2,c} \quad \text{.....(10)}$$

where, $\theta_{1,c}$ and $\theta_{2,c}$ are the corresponding values of θ_1 and θ_2 when reaction (I) finished.

The definitions of the dimensionless parameters appearing in Eqs. (5) to (10) are given in Eqs. (11), in which the subscript i stands for "1" and "2", respectively.

$$\xi=r_1/r_o\,, \qquad \zeta=r_2/r_o \quad \text{.....(11-a)}$$

$$\theta_i=[b_i M_i k_i(c_b-c_i^*)t]/[\rho_{si}(1-\varepsilon_i)x_{si}r_o] \quad \text{.....(11-b)}$$

$$\gamma_i=(1+K_i)/K_i \quad \text{.....(11-c)}$$

$$\phi_i^*=c_i^*/c_b \quad \text{.....(11-d)}$$

The overall reduction conversion can be expressed by Eq. (12).

$$x=1/3(1-\xi^3)+2/3(1-\zeta^3) \quad \text{.....(12)}$$

Where, the λ_f, λ_{d1}, λ_{c1}, λ_{d2} and λ_{c2} stand for the resistance of each step concerned, and their expressions are listed below.

Resistance of mass transfer through the stagnant gaseous film around the pellet:

$$\lambda_f=1/k_f \quad \text{.....(13)}$$

Resistance of gaseous species' diffusing through the second product layer ($Fe+TiO_2$):

$$\lambda_{d2}=\frac{r_o}{D_{e2}}\frac{1-\zeta}{\zeta} \quad \text{.....(14-a)}$$

Resistance of the intrinsic chemical reaction (II):

$$\lambda_{c2}=\frac{K_2}{k_2(1+K_2)}\frac{1}{\zeta^2} \quad \text{.....(14-b)}$$

Resistance of the diffusion of gaseous species through the first product layer ($FeTiO_3+TiO_2$):

$$\lambda_{d1}=\frac{r_o}{D_{e1}}\frac{\zeta-\xi}{\zeta\xi} \quad \text{.....(15-a)}$$

Resistance of the intrinsic chemical reaction (I):

$$\lambda_{c1}=\frac{K_1}{k_1(1+K_1)}\frac{1}{\xi^2} \quad \text{.....(15-b)}$$

3.3. Kinetic Parameters

3.3.1. Rate Constants and Effective Diffusivities

Because of the two-interface characteristics, it is easy to understand that the reduction data can not be successfully interpreted with one-interface kinetic model. In order to analyze the reduction kinetics numerically with the two-interface kinetic model, the kinetic parameters appearing in the equations must be known in advance. They were determined in the following ways.

(a) Parameters Concerned with Reaction (II)

After reaction (I) finished, the reaction interface position of reaction (II), ζ, can be derived from Eq. (12).

$$\zeta=[1-(3x-1)/2]^{1/3} \quad \text{.....(12-a)}$$

If reaction (I) finished at time t_c, a modified one-interface kinetic model describing the relation between ζ and t was derived as Eq. (16).

$$(t-t_c)/(\zeta_c-\zeta)=A_2+B_2[3(\zeta+\zeta_c)-2(\zeta^2+\zeta\zeta_c+\zeta_c^2)] \quad \text{.....(16)}$$

where ζ_c is the reaction interface position of reaction (II) at time t_c, and A_2 and B_2 are constants expressed by Eqs. (17).

$$A_2=\frac{\rho_{s2}(1-\varepsilon_2)x_{s2}r_o}{b_2M_2(c_b-c_2^*)}\frac{r_o}{6D_{e2}} \quad \text{.....(17-a)}$$

$$B_2=\frac{\rho_{s2}(1-\varepsilon_2)x_{s2}r_o}{b_2M_2(c_b-c_2^*)}\frac{K_2}{k_2(1+K_2)} \quad \text{..... (17-b)}$$

According to least square method, the best fit coefficients A_2 and B_2 were determined with experimental data by substituting Eq. (12-a) into Eq. (16), consequently, the rate constant of reaction (II), k_2, and the effective diffusivity of the gaseous species through the product (Fe+TiO_2) layer, D_{e2}, were obtained from Eqs. (17).

(b) Parameters Concerned with Reaction (I)

During the initial stage of the reduction, the relation between the position of the first interface and reduction conversion can be expressed by Eq. (12-b).

$$\xi=\{1-[3x-2(1-\zeta^3)]\}^{1/3} \quad \text{..... (12-b)}$$

Substituting the values of x at time t and the corresponding value of ζ determined according to Eq. (16) into Eq. (12-b), a group data of ξ versus reaction time t was obtained. According to the mixed control kinetic model expressed by Eqs. (18) and (19), the kinetic parameters k_1 and D_{e1} of reaction (I) were calculated.

$$t/(1-\xi)=A_1+B_1(1+\xi-2\xi^2) \quad \text{.....(18)}$$

where A_1 and B_1 stand for:

$$A_1=\frac{\rho_{s1}(1-\varepsilon_1)x_{s1}r_o}{b_1M_1(c_2^*-c_1^*)}\frac{r_o}{6D_{e1}} \quad \text{.....(19-a)}$$

$$B_1=\frac{\rho_{s1}(1-\varepsilon_1)x_{s1}r_o}{b_1M_1(c_2^*-c_1^*)}\frac{K_1}{k_1(1+K_1)} \quad \text{..... (19-b)}$$

(c) Parameters Concerned with the Reduction of Unoxidized Ilmenite Pellets

Because all of the three kinds of natural ilmenite ores contained small amount of ferric material,[15] the reduction of unoxidized pellets also included the conversion of the ferric material into ferrous material besides the main reaction (II). The method of analyzing the reduction kinetics of unoxidized pellets was similar to that used for interpreting the kinetics of reaction (II) of the reduction of preoxidized pellets.

Typical results analyzed according to the aforementioned method are illustrated in **Fig. 6**, which shows that only the two-interface kinetic model (g_1 *vs.* f_1 and g_2 *vs.* f_2) successfully interprets the reduction kinetics of preoxidized ilmenite pellet, however, the one-interface kinetic model (g *vs.* f) does not fit the experimental results because the data do not fall into a straight line.

3.3.2. Temperature Dependence

All of the Arrhenius equations of reaction rate constants, effective diffusivities and the structural parameters defined by Eq. (20) were summarized in **Tables**

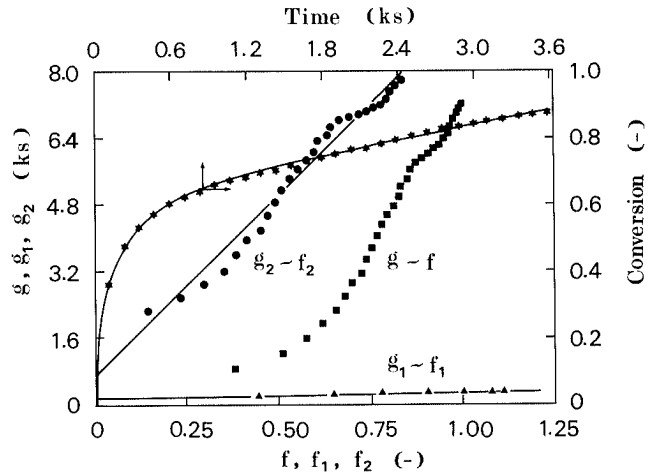

Fig. 6. Comparison of the validity of the two-interface kinetic model with that of the one-interface kinetic model.
$g=t/F$ $\quad f=3F-2F^2$
$g_1=t/(1-\xi)$ $\quad f_1=1+\xi-2\xi^2$
$g_2=(t-t_c)/(\zeta_c-\zeta)$ $\quad f_2=3(\zeta+\zeta_c)-2(\zeta^2+\zeta\zeta_c+\zeta_c^2)$

Table 3. Temperature dependence of the kinetic parameters measured with unoxidized pellets.

Pellets	Intrinsic chemical reaction rate constant, k ($m\cdot s^{-1}$)	Intrapellet diffusivity, D_e ($m^2\cdot s^{-1}$)	Structural parameter, (ε/τ) (−)
ACP	$3.11\times10^5\exp[-167\times10^3/(RT)]$	$9.29\times10^{-3}\exp[-59.0\times10^3/(RT)]$	$1.93\exp[-42.6\times10^3/(RT)]$
CCP	$4.36\times10^7\exp[-221\times10^3/(RT)]$	$3.05\times10^{-4}\exp[-17.3\times10^3/(RT)]$	$0.063\exp[-0.881\times10^3/(RT)]$
MCP	$2.84\times10^3\exp[-133\times10^3/(RT)]$	$0.067\exp[-71.7\times10^3/(RT)]$	$14.0\exp[-55.3\times10^3/(RT)]$

Table 4. Temperature dependence of the kinetic parameters measured with pellets preoxidized at 1073 K.

Pellets	Intrinsic chemical reaction rate constant, k ($m\cdot s^{-1}$)	Intrapellet diffusivity, D_e ($m^2\cdot s^{-1}$)	Structural parameter, (ε/τ) (−)
ACP	$k_1=5.76\times10^7\exp[-186\times10^3/(RT)]$ $k_2=6.84\exp[-66.2\times10^3/(RT)]$	$D_{e1}=1.72\times10^{-3}\exp[-43.2\times10^3/(RT)]$ $D_{e2}=1.58\times10^{-4}\exp[-7.97\times10^3/(RT)]$	$(\varepsilon/\tau)_1=0.387\exp[-27.7\times10^3/(RT)]$ $(\varepsilon/\tau)_2=3.56\times10^{-2}\exp[7.59\times10^3/(RT)]$
CCP	$k_1=3.15\times10^4\exp[-123\times10^3/(RT)]$ $k_2=658\exp[-107.5\times10^3/(RT)]$	$D_{e1}=2.62\times10^{-5}\exp[1.66\times10^3/(RT)]$ $D_{e2}=1.08\times10^{-3}\exp[-26.3\times10^3/(RT)]$	$(\varepsilon/\tau)_1=5.91\times10^{-3}\exp[17.2\times10^3/(RT)]$ $(\varepsilon/\tau)_2=0.245\exp[-10.7\times10^3/(RT)]$
MCP	$k_1=2.03\exp[-40.7\times10^3/(RT)]$ $k_2=2.67\times10^3\exp[-119\times10^3/(RT)]$	$D_{e1}=1.96\times10^{-5}\exp[7.72\times10^3/(RT)]$ $D_{e2}=1.13\times10^{-2}\exp[-47.5\times10^3/(RT)]$	$(\varepsilon/\tau)_1=11.2\exp[-43.7\times10^3/(RT)]$ $(\varepsilon/\tau)_2=2.55\exp[-31.9\times10^3/(RT)]$

Table 5. Temperature dependence of the kinetic parameters measured with pellets preoxidized at 1273 K.

Pellets	Intrinsic chemical reaction rate constant, k ($m \cdot s^{-1}$)	Intrapellet diffusivity, D_e ($m^2 \cdot s^{-1}$)	Structural parameter, (ε/τ) (−)
ACP	$k_1 = 2.58 \exp[-41.5 \times 10^3/(RT)]$ $k_2 = 3.36 \times 10^6 \exp[-177 \times 10^3/(RT)]$	$D_{e1} = 5.40 \times 10^{-3} \exp[-45.9 \times 10^3/(RT)]$ $D_{e2} = 5.33 \times 10^{-5} \exp[2.36 \times 10^3/(RT)]$	$(\varepsilon/\tau)_1 = 1.21 \exp[-30.2 \times 10^3/(RT)]$ $(\varepsilon/\tau)_2 = 1.20 \times 10^{-2} \exp[17.9 \times 10^3/(RT)]$
CCP	$k_1 = 0.334 \exp[-21.8 \times 10^3/(RT)]$ $k_2 = 4.05 \times 10^4 \exp[-133 \times 10^3/(RT)]$	$D_{e1} = 3.58 \times 10^{-2} \exp[-64.0 \times 10^3/(RT)]$ $D_{e2} = 2.94 \times 10^{-4} \exp[-11.3 \times 10^3/(RT)]$	$(\varepsilon/\tau)_1 = 8.17 \exp[-48.6 \times 10^3/(RT)]$ $(\varepsilon/\tau)_2 = 6.64 \times 10^{-2} \exp[4.25 \times 10^3/(RT)]$
MCP	$k_1 = 3.35 \times 10^2 \exp[-85.8 \times 10^3/(RT)]$ $k_2 = 18.5 \exp[-76.3 \times 10^3/(RT)]$	$D_{e1} = 1.05 \times 10^{-6} \exp[34.2 \times 10^3/(RT)]$ $D_{e2} = 1.43 \times 10^{-3} \exp[25.2 \times 10^3/(RT)]$	$(\varepsilon/\tau)_1 = 2.38 \times 10^{-4} \exp[49.8 \times 10^3/(RT)]$ $(\varepsilon/\tau)_2 = 0.323 \exp[-9.63 \times 10^3/(RT)]$

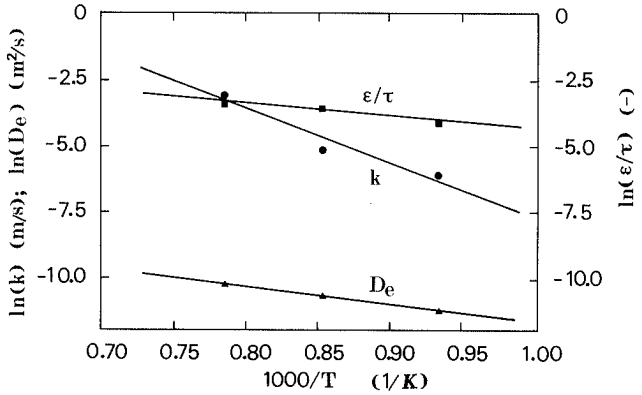

Fig. 7. Temperature dependence of rate constant, effective diffusivity and the structural parameter of reduced layer for the reduction of unoxidized ACP.

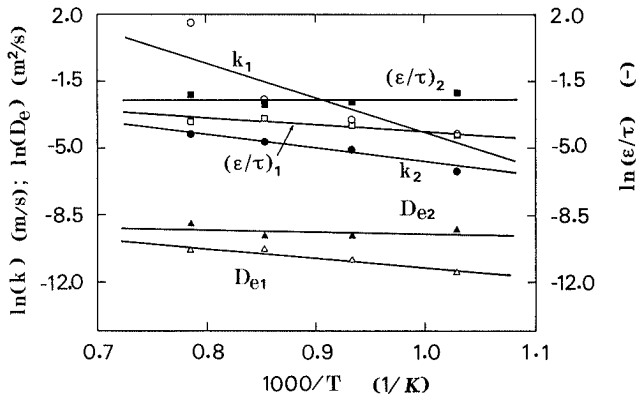

Fig. 8. Temperature dependence of rate constants, effective diffusivities and the structural parameters of reduced layers for the reduction of ACP preoxidized at 1073 K.

3, **4** and **5**. The molecular diffusivity of the H_2–H_2O system, D_{12}, included in Eq. (20) was estimated with Chapman–Enskog's equation.[16] Representative results are shown in **Figs. 7**, **8** and **9**.

$$\varepsilon/\tau = D_e/D_{12} \quad \text{.....(20)}$$

The difference in the kinetic parameters measured with different kinds of pellets was mainly contributed to the difference in their original composition. For the pellets made of same ilmenite ore, the difference in the kinetic parameters measured with the unoxidized ilmenite pellets and the preoxidized ilmenite pellets was mainly caused by the preoxidation which not only changed the mineral composition of the pellets but also reformed their microstructure.[9]

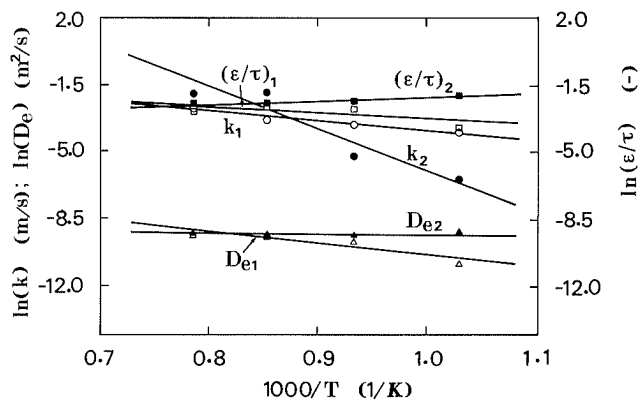

Fig. 9. Temperature dependence of rate constants, effective diffusivities and the structural parameters of reduced layers for the reduction of ACP preoxidized at 1273 K.

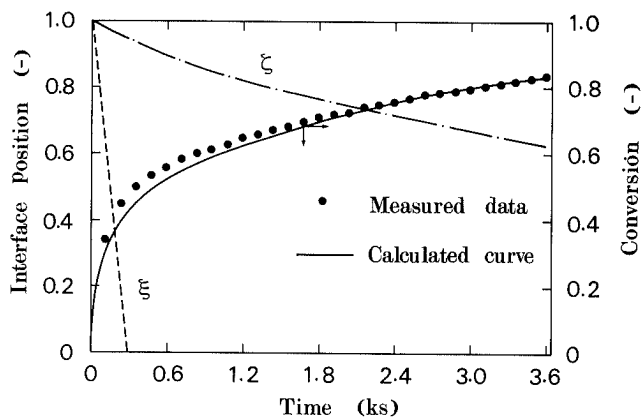

Fig. 10. Comparison of the measured fractional conversion of the reduction (1073 K) of ACP preoxidized at 1273 K with the calculated ones.

3.3.3. Mass Transfer Coefficient

The mass transfer coefficient of gaseous species through the stagnant gaseous film around the pellet, k_f, was estimated according to Ranz–Marshall's equation.[17]

$$N_{Sh} = 2.0 + 0.6 N_{Rep}^{1/2} N_{Sc}^{1/3} \quad \text{.....(21)}$$

where $N_{Sh} = k_f d_p/D_{12}$, $N_{Rep} = u d_p/\nu$ and $N_{Sc} = D_{12}/\nu$ are Sherwood number, particle-Reynolds number and Schmidt number, respectively.

3.4. Numerical Analysis

The two differential equations of the two-interface kinetic model, Eqs. (5) and (6), were solved numerically with their corresponding initial conditions and the kinet-

ic parameters obtained above by means of fourth order Runge–Kutta–Gill's method. Substituting the values of the position of the two interfaces into Eq. (12), the overall conversion was found. **Figure 10** compares typical results of calculation with that of measurement, showing that their agreement is satisfactory. Similar results were also obtained for CCP and MCP. Figure 10 also depicts the progress of the two reaction interfaces during reduction, showing that reaction (I) almost finished within several minutes and the overall reduction mainly consisted of reaction (II).

4. Discussion of Rate-controlling Step

4.1. Reduction of Preoxidized Ilmenite Pellets

Usually the rate-controlling step was evaluated in terms of its resistance fraction.[18] In the case of multi-interface system, the intrinsic chemical reaction and the intrapellet diffusion proceed simultaneously in a parallel-series manner.[19] This makes it more difficult to analyze the relative importance of each step in terms of the resistance fraction. In the following discussion, the contribution of each step concerned with reactions (I) and (II) will be discussed separately and the relative importance of the two reactions will be described with two parameters R_1 and R_2.

In the course of reduction, a part of the H_2 diffused through the second product layer took part in reaction (II) at the second interface and the rest continued its diffusion to access the first interface where reaction (I) took place. At steady state, the mass fraction of the H_2 participating reaction (I) must equal the ratio of the rate of reaction (I) to that of the overall reduction and similar equality holds true for the rest part of H_2 and reaction (II).

If we designated the rate ratios of reactions (I) and (II) to that of the overall reduction as R_1 and R_2, another form of the rate expressions for reaction (I) and (II) was derived as follows.

$$v_1=\frac{c_b-c_1^*}{(\lambda_f+\lambda_{d2})/R_1+(\lambda_{d1}+\lambda_{c1})} \quad \text{.....(22)}$$

$$v_2=\frac{c_b-c_2^*}{(\lambda_f+\lambda_{d2})/R_2+\lambda_{c2}} \quad \text{.....(23)}$$

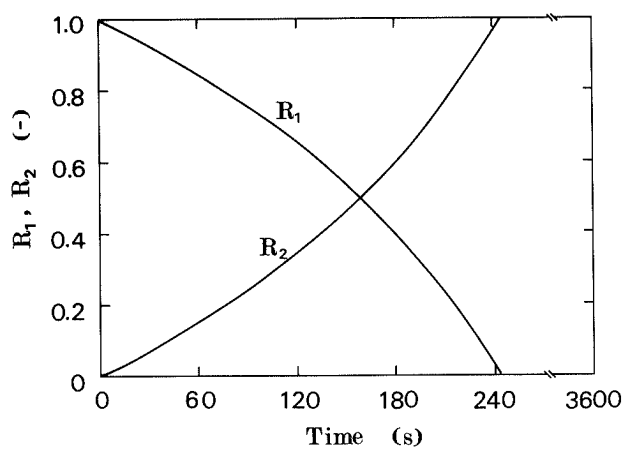

Fig. 11. Contribution of reactions (I) and (II) to the overall reduction (1 173 K) of ACP preoxidized 1 273 K.

where

$$R_1=v_1/(v_1+v_2) \quad \text{and} \quad R_2=v_2/(v_1+v_2) \quad \text{.....(24)}$$

Typical values of R_1 and R_2 throughout the reduction were illustrated in **Fig. 11** showing that the contribution of reaction (I) could not be neglected in the initial stage.

If the denominators of Eqs. (22) and (23) are defined as the total resistance of reactions (I) and (II), and they are designated as Λ_1 and Λ_2, respectively, the resistance fraction of each step concerned with reactions (I) and (II) can be expressed as follows.

Resistance fraction of mass transfer through the stagnant gaseous film for reactions (I) and (II):

$$R_{f,1}=(\lambda_f/R_1)/\Lambda_1 \quad \text{.....(25-a)}$$

$$R_{f,2}=(\lambda_f/R_2)/\Lambda_2 \quad \text{.....(25-b)}$$

Resistance fraction of the diffusion of gaseous species through the second product layer for reactions (I) and (II):

$$R_{d2,1}=(\lambda_{d2}/R_1)/\Lambda_1 \quad \text{.....(26-a)}$$

$$R_{d2,2}=(\lambda_{d2}/R_2)/\Lambda_2 \quad \text{.....(26-b)}$$

Resistance fraction of gaseous species' diffusing through the first product layer:

$$R_{d1}=\lambda_{d1}/\Lambda_1 \quad \text{.....(27)}$$

Resistance fraction of the intrinsic chemical reactions (I) and (II):

$$R_{c1}=\lambda_{c1}/\Lambda_1 \quad \text{.....(28-a)}$$

$$R_{d2}=\lambda_{c2}/\Lambda_2 \quad \text{.....(28-b)}$$

A typical result is illustrated in **Figs. 12** and **13**, which show that reaction (I) was mainly controlled by both the gas diffusion through the first product layer and the intrinsic chemical reaction and reaction (II) was mainly controlled by the gas diffusion through the second product layer.

4.2. Reduction of Unoxidized Ilmenite Pellets

In the case of the reduction of unoxidized pellets, the reacting pellet was mainly a one-interface system. The

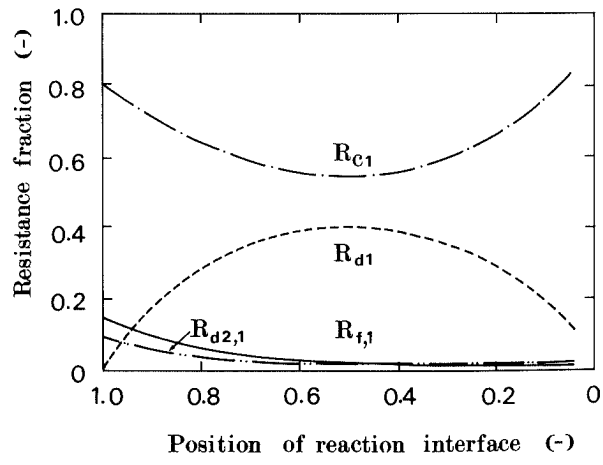

Fig. 12. Resistance fraction of each step concerning reaction (I) during the reduction (1 173 K) of ACP preoxidized at 1 073 K.

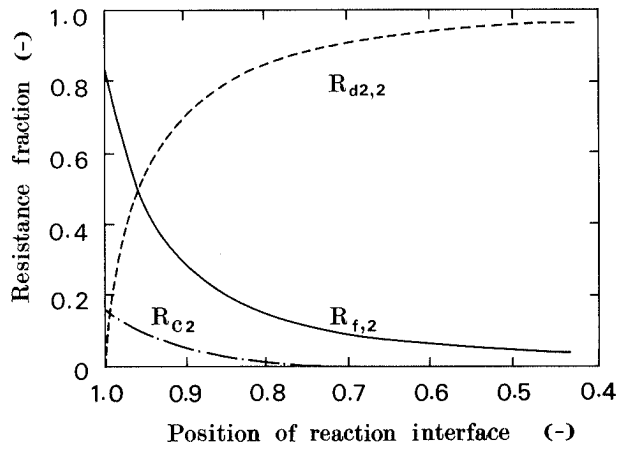

Fig. 13. Resistance fraction of each step concerning reaction (II) during the reduction (1 173 K) of ACP preoxidized at 1 073 K.

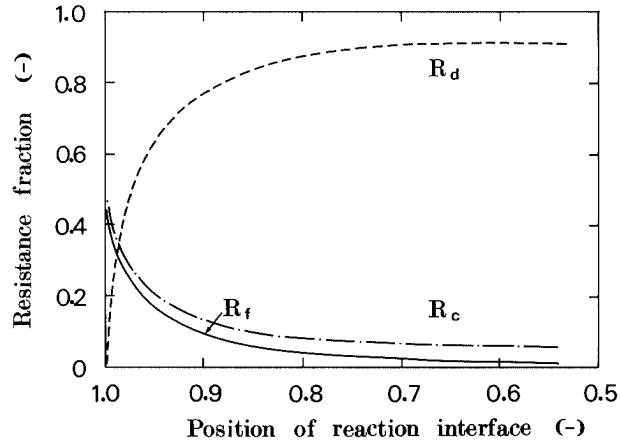

Fig. 14. Resistance fraction of each step during the reduction of unoxidized ACP at 1 173 K.

resistance fraction of each step was evaluated as follows.

Resistance fraction of mass transfer through the stagnant gaseous film:

$$R_f = \lambda_f / \Lambda \quad \text{.....(29)}$$

Resistance fraction of intrapellet diffusion:

$$R_d = \lambda_{d2} / \Lambda \quad \text{.....(30)}$$

Resistance fraction of intrinsic chemical reaction:

$$R_c = \lambda_{c2} / \Lambda \quad \text{.....(31)}$$

where Λ is the total resistance:

$$\Lambda = \lambda_f + \lambda_{d2} + \lambda_{c2} \quad \text{.....(32)}$$

Typical results are presented in **Fig. 14**, which shows that the reduction rate of unoxidized ilmenite pellet was mainly controlled by the intrapellet diffusion of gaseous species except in the initial period.

5. Conclusions

(1) Preoxidation of the three kinds of cement-bonded ilmenite pellets accelerated their subsequent reduction.

(2) Macroscopically, the reduction of cement-bonded ilmenite pellets proceeded topochemically.

(3) Two-interface kinetic model applied to the interpretation of the hydrogen reduction kinetics of preoxidized ilmenite pellets; As a derivative of the two-interface kinetic model, the modified one-interface kinetic model was suitable for analyzing the kinetic behavior of the reduction of unoxidized natural ilmenite pellets. The reduction rate constants and the effective diffusivities were summarized in Tables 3, 4 and 5.

(4) Both the intrapellet diffusion of gaseous species and the intrinsic chemical reaction played an important role during reaction (I). Reaction (II) was mainly controlled by the diffusion of gaseous species through product layer. The reduction of unoxidized pellets was predominated by the intrapellet diffusion of gaseous species except in the initial period.

Acknowledgment

The authors want to express their sincere thanks to the staff of Tohkem Products Corporation for their supplying the natural ilmenite samples.

Nomenclature

b_1, b_2: stoichiometric coefficients of the solid reactant in reactions (I) and (II) (—)
c_b: concentration of H_2 in the bulk gaseous phase ($mol \cdot m^{-3}$)
c_1^*, c_2^*: equilibrium concentrations of H_2 calculated according to reactions (I) and (II) ($mol \cdot m^{-3}$)
d_p: pellet diameter (m)
D_{e1}, D_{e2}: effective diffusivities of gaseous species through the first product layer and the second product layer ($m^2 \cdot s^{-1}$)
F: $F = 1-(1-x)^{1/3}$ (—)
k_1, k_2: rate constants of reactions (I) and (II) ($m \cdot s^{-1}$)
k_f: mass transfer coefficient of gaseous species through the stagnant gaseous film ($m \cdot s^{-1}$)
K_1, K_2: equilibrium constants of reactions (I) and (II), respectively (—)
M_1, M_2: molar weight of Fe_2O_3 and $FeTiO_3$ ($kg \cdot mol^{-1}$)
r_o: pellet radius (m)
R: gas constant ($J \cdot K^{-1} \cdot mol^{-1}$)
t: reaction time (s)
t_c: reaction time when reaction (I) finished (s)
T: absolute temperature (K)
u: gas flow velocity ($m \cdot s^{-1}$)
v_1, v_2: reaction rates of reactions (I) and (II) ($mol \cdot s^{-1}$)
x: reduction conversion (—)
x_{s1}, x_{s2}: mass fraction of Fe_2O_3 and $FeTiO_3$ in the pellet (—)
γ_1, γ_2: $\gamma_1 = (1+K_1)/K_1$; $\gamma_2 = (1+K_2)/K_2$ (—)
ε: porosity of the pellet (—)
$\varepsilon_1, \varepsilon_2$: porosity of the pellets preoxidized and unoxidized respectively (—)
ζ: dimensionless position of the second reaction interface, r_2/r_o (—)
θ_1, θ_2: dimensionless reaction time of reaction (I) and (II) (—)
ν: kinematic viscosity ($m^2 \cdot s^{-1}$)
ξ: dimensionless position of the first reaction

interface, r_1/r_o (—)

ρ_{a1}, ρ_{a2}: apparent density of preoxidized pellet and that of unoxidized pellet ($kg \cdot m^{-3}$)

ρ_{s1}, ρ_{s2}: true density of preoxidized pellet and that of unoxidized pellet ($kg \cdot m^{-3}$)

τ: tortuosity factor of the reduced layer (—)

REFERENCES

1) R. H. Walsh, H. W. Hockin, D. R. Brandt, P. L. Dietz and P. R. Girardot: *Trans. Metall. Soc. AIME*, **218** (1960), 994.
2) M. I. EL-Guindy and W. G. Davenport: *Metall. Trans.*, **1** (1970), 1729.
3) K. Tittle and E. Foley: *Trans. Instn. Min. Metall.*, **82** (1973), C135.
4) I. E. Grey, D. G. Jones and A. F. Reid: *Trans. Instn. Min. Metall.*, **82** (1973), C151.
5) D. G. Jones: *Trans. Instn. Min. Metall.*, **82** (1973), C186.
6) I. E. Grey and A. F. Reid: *Trans. Instn. Min. Metall.*, **83** (1974), C39.
7) I. E. Grey, A. F. Reid and D. G. Jones: *Trans. Instn. Min. Metall.*, **83** (1974), C105.
8) D. G. Jones: *Trans. Instn. Min. Metall.*, **83** (1974), C1.
9) R. Merk and C. A. Pickles: *Can. Metall. Q.*, **27** (1988), 179.
10) M. C. L. Patterson and J. Cameron: *Trans. Instn. Min. Metall.*, **94** (1985), C215.
11) S. K. Gupta, V. Rajakumar and P. Grieveson: *Metall. Trans.*, **18B** (1987), 713.
12) D. Bhogeswara Rao and M. Rigaud: *Hight Temp. Sci.*, **6** (1974), 323.
13) S. K. Gupta, V. Rajakumar and P. Grieveson: *Can. Metall. Q.*, **29** (1990), 43.
14) J.-L. Fihey, F. Ajersch and E. A. Dancy: *Can. Metall. Q.*, **18** (1979), 419.
15) K. Sun, M. Ishii, R. Takahashi and J. Yagi: *ISIJ Int.*, **32** (1992), 489.
16) R. B. Bird, W. E. Stewart and E. N. Lightfoot: Transport Phenomena, John Wiley & Sons, Inc., New York, (1960), 511.
17) W. E. Ranz and W. R. Marshall, Jr.: *Chem. Eng. Prog.*, **48** (1952), 141, 173.
18) A. Moriyama, J. Yagi and I. Muchi: *Trans. Iron Steel Inst. Jpn.*, **7** (1967), 271.
19) R. H. Spitzer, F. S. Manning and W. O. Philbrook: *Trans. Met. Soc. AIME*, **236** (1966), 1715.